SSC23-WIII-05

Design of a Scientific-grade Multispectral Imager for Nanosatellites

Joosep Kivastik, Silvar Muru, Meelis Pihlap, Hans Hubert Sams, Madis Kaspar Nigol, Hendrik Ehrpais, Mihkel Pajusalu
Tartu Observatory, University of Tartu
Observatooriumi 1, Tõravere, Estonia; +372 737 4510
joosep.kivastik@ut.ee

ABSTRACT

Applications in agriculture, land-cover change, and vegetation phenology, to name a few, would benefit from more frequent high-quality remote sensing data. However, "Landsat-class" satellites are too expensive for such applications. Therefore, there is a need to augment larger Earth observation satellites with nanosatellites that use scientific-grade imaging instruments. This paper presents the design for the scientific-grade multispectral imager Theia. It is designed for a 5% radiometric accuracy at a ground sampling distance of 33 m at a 650 km orbit while keeping the modulation transfer function above 0.13 at the Nyquist frequency. The camera has reflective optics with an aluminium optomechanical design to mitigate stress from thermal expansion. Furthermore, the optical path is covered with a mix of black anodization and Acktar Magic Black to suppress stray-light. The sCMOS sensor is back-side illuminated to increase the radiometric quality of the instrument. Furthermore, the imager has a post-launch calibration system for continuous monitoring of the instrument's quality. The performance is achieved while fitting inside 0.6 CubeSat Units and weighing about 600 g. However, a trade-off between the modulation transfer function and radiometric quality is presented. Such an imager, when deployed on numerous nanosatellites, can enable new kinds of missions that are otherwise too costly. The project is funded by the European Space Agency.

Introduction

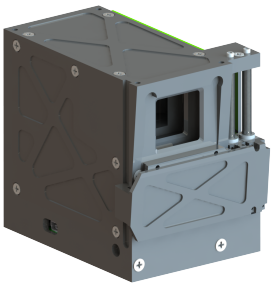

Figure 1: Rendering of Theia.[1]

The University of Tartu Tartu Observatory has designed Theia (Figure 1) in cooperation with the European Space Agency. The imager achieves a radiometric accuracy of 5%, while keeping the modulation transfer function (MTF) above 0.13 at the Nyquist frequency of the sensor (77 lp/mm) and having an unsmeared ground-sampling distance of 33 m at a 650 km orbit. These specifications make the camera suitable for quantitative remote sensing studies.

Instruments like Theia could be companions to larger "Landsat-class" satellites. Even though more large remote sensing satellites are being built, they are still expensive,[2] and therefore, there will always be an issue with the temporal frequency of data samples. So, suppose we have a constellation of scientific-grade imagers that can supply complementary data that is worse but comparable to larger satellites. In that case, we can have higher frequency monitoring, which is already needed for different applications in, for example, agriculture,[3] land-cover change,[4] and vegetation phenology.[5] Furthermore, having a constellation of accurate imagers also allows us to study the reflection distribution functions of objects, as it is possible to image the same object from multiple angles simultaneously.

Theia images in two spectral bands simultaneously by splitting the optical bath into two with a beam splitter. Due to the reflective optics, the imager is also free of chromatic aberration, making it easier for the user to configure the camera to new custom bands. Moreover, the camera adheres to the CubeSat standard,[6] making integration to the used satellite platform easier. More specifically, it fits inside 0.6U and weighs about 600 g. Lastly, Theia also has an onboard calibration module that can characterise the camera's performance degradation throughout its lifespan. Currently (as of June 2023), the prototype is manufactured and in testing, where

the analysis and design are being validated and the calibration procedure tested.

Optics

This optics section is a short summary of our optical design paper.[1]

The imager is small, lightweight and has to be able to work at different spectral bands. The prototype instrument was designed to measure the normalized difference vegetation index.[7] This means that the instrument has to be able to image in the red and near-infrared (NIR) spectra, which were chosen as 665 nm and 864 nm, respectively.

Radiometric Budget

The radiometric budget was analysed in parallel with the instrument's optical design. The analysis resulted in an optimised camera layout and cost-effective part selection. A more thorough analysis of the radiometry of the instrument can be seen at.[1] However, the main takeaways are listed in Table 1.

Table 1: Radiometric Budget[1]

Variable	665 nm	864 nm
Pixel Pitch	6.5 μm	
Integration Time	0.7 ms	
Orbit altitude	650 km	
Top of the atmosphere radiance	20 $\frac{W}{sr \cdot m^2 \cdot \mu m}$	100 $\frac{W}{sr \cdot m^2 \cdot \mu m}$
SNR	31	48
SNR at 5 samples	70	107

We assumed that to achieve at least a 5% radiometric accuracy, we would need a raw signal-to-noise-ratio (SNR) of at least 50 with some extra margin. As can be seen from Table 1, we cannot reach this with one sample per object. However, if we sample the same object multiple times, then the noise decreases with the square root of the number of samples. Therefore, given our sensor size, orbital and optical parameters at five samples, we can achieve SNRs of 70 and 107 for the 665 nm and 864 nm spectral bands, respectively.[1]

Optical Design

We used a classical unobscured three-mirror anastigmat design[8] with aspherical aluminium mirrors to correct for the main optical aberrations. Because the camera uses reflective optics, it has no chromatic aberration, simplifying the change of spectral bands. Moreover, the fully aluminium design mitigates the stress caused by thermal expansion as the coefficients of thermal expansion are the same for the mirrors and their surrounding structure. Also, aluminium is a durable low-density metal with much space heritage.[1]

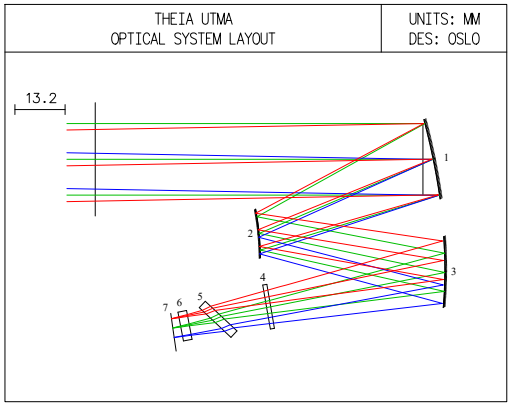

Figure 2: NIR path of the optical design: 1 – primary mirror, 2 – secondary mirror, 3 – tertiary mirror, 4 – dichroic mirror, 5 – compensator for the dichroic mirror, 6 – 864 nm bandpass filter, 7 – image plane.[1]

Table 2: Main Optical Parameters[1]

Parameter	Value
Effective focal length	130.5 mm
F-number	4.91
Full field-of-view	2.1° x 2.7° (rectangular)

The optics layout can be seen in Figure 2, and the main parameters can be seen in Table 2. After the tertiary mirror, the optical path is split into two by a fused silica beam splitter. The NIR light gets refracted. However, the high angle of the beam splitter creates astigmatism. To compensate for this, a fused silica element is placed behind the beam splitter, angled in the perpendicular direction cancelling the astigmatism [9, p. 92]. In front of both sensors, there are band-pass filters. The band-pass filters and the compensator have an anti-reflective coating on the sides of the sensor that helps mitigate ghosting by letting the light reflected off the sensor dissipate within the baffling system.[1]

Optical Performance

The main design driver of the optical performance was to keep the design diffraction limited, meaning that the optics would be limited by physics

and not by design. According to the Marechal ciretrion,[10] if the root-mean-square wavefront error is smaller than 0.07 wavelengths (λ). This was achieved throughout the field-of-view of both sensors while also considering the manufacturing tolerances. A more thorough analysis can be seen at.[1]

Furthermore, resolution is only a part of the quality equation. It is also essential to have a sufficient modulation transfer function, which characterizes the contrast of the images. On Sentinel-2, the MTF is kept between 0.15 and 0.3 depending on the specific spectral band.[11] Therefore, we aimed to achieve at least 0.13 at the Nyquist frequency of the sensor. The design's MTF can be seen in Figure 3.

A Monte Carlo analysis was done with Optics Software for Layout (OSLO).[12] Based on 1000 configurations, there is a 99% probability for the 864 nm band and a 95% probability for the 665 nm band that the resultant MTF will be above 0.13. However, because the analyses had to be done separately for the spectral bands, this does not guarantee an MTF above 0.13 at the Nyquist frequency. Furthermore, taking the satellite's motion into account then, it is likely that the MTF will be below 0.13 for the red band. Therefore, if the MTF is the limiting factor for an application, then a trade-off between the SNR and MTF, a trade-off between MTF in different axes or using a deblurring algorithm could be considered. More thorough information and analysis are available at.[1]

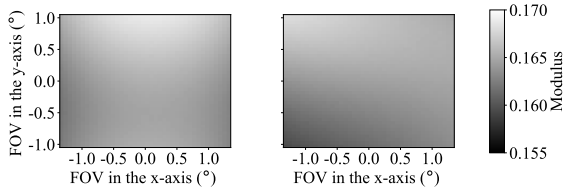

Figure 3: MTF for 77 lp/mm for the 665 nm band (left) and 864 nm band (right).[1]

Stray Light

The three-mirror design inherently suppresses the stray light in the instrument, as the sensors are deep inside the instrument. However, care was taken such that out-of-field-of-view light does not directly fall on the secondary mirror. Furthermore, the inside of the optical path is covered with a mix of black anodization and Acktar's Magic Black.[13] The choice of how to coat the inside was based on stray-light analysis. Figure 4 shows the baffling system's three sections.[1]

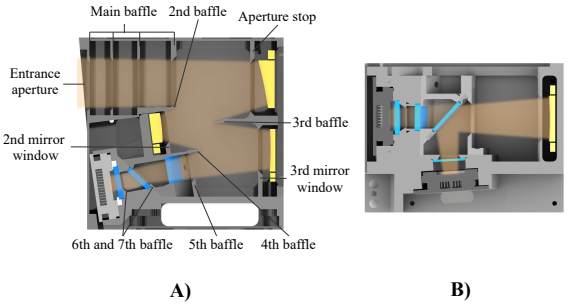

Figure 4: Baffling system of Theia.[1]

In the stray-light analysis, we took into account the following:

- scattering from surface roughness and contamination,
- unwanted reflections inside the instrument, and
- out-of-field-of-view light entering the system.

The Monte Carlo ray tracing analysis done with TracePro[14] showed that if we have a 2 nm root-mean-square surface roughness of the mirrors and particle contamination of around 0.7% and an anti-reflective coating on the refractive elements that keep the reflectance below 0.5% in both bands, then we would have a stray-light of 1.2% for the red band and 1% for the NIR band. Therefore, considering Table 1, we would have the resultant SNRs of 62 and 92 for the red and NIR bands, respectively. The resultant SNRs give the camera enough margin to achieve a 5% radiometric accuracy.[1]

Calibration Module

A post-launch calibration module has been added to the camera to sustain the instrument's accuracy and monitor its degradation. A calibration system is standard on bigger Earth observation satellites such as Sentinel-2;[15] however, it has yet to be implemented for a nanosatellite instrument. So, after the instrument's characterisation and calibration on Earth, the instrument performs a calibration as soon as possible after launch. The calibration consists of two parts. Firstly, a diffuser is slid in front of the optical path, and the imager takes images of the Sun. The diffuser creates a uniform grey image on the sensor. This is used for flat-fielding. Secondly, an aluminium shutter is slid in front of the optical path, which allows us to capture dark frames. Therefore, we can measure the dark noise environment. The different calibration modes can be seen in Figure 5.[1,16]

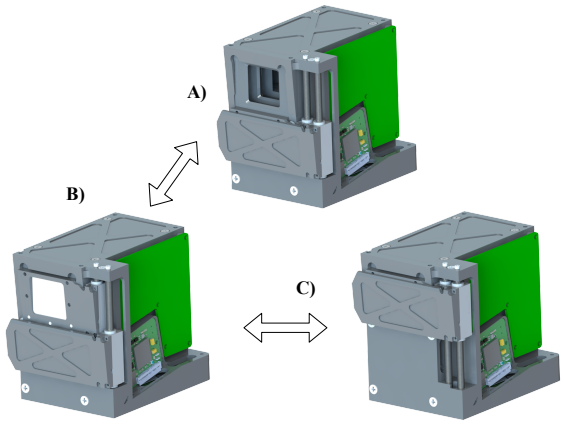

Figure 5: Calibration module.[1]

Mechanics

The mechanical enclosure was designed to house the optical design, electronics and external calibration unit. In the design process, all manufacturing and optical system limitations were considered. This concluded in a structural system design where the frame has sufficient strength and rigidity while providing enough space and surfaces to help to baffle stray light to increase the radiometric quality. The main body and the Image Detection Module are milled out of a solid 7075-T6 aluminium[17] block, giving the structure fewer points of failure and higher accuracy. The 7075-T6 was chosen for its high strength-to-density ratio and availability by the manufacturer. The trade-off for this material is its higher cost. The final prototype of the EOI can be seen in Figure 6.

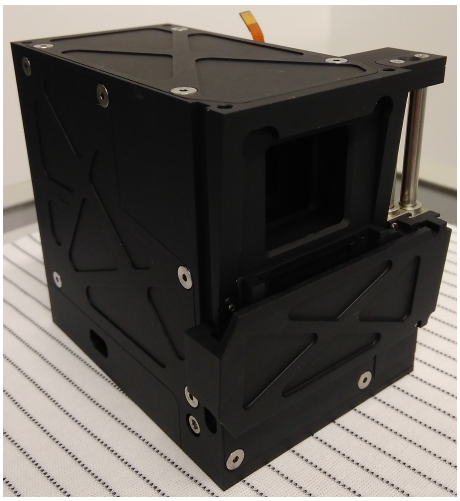

Figure 6: EOI final prototype.

Mirror Fine Alignment

To mitigate any manufacturing or coating imperfections that may cause mirror misalignments, a dynamic fine adjustable mounting system was considered to solve this issue. The chosen system for this application is a four-point kinematic mount, as seen in Figure 7. It uses four M2.5 set screws with 0.2 mm pitch from Thorlabs.[18] These allow the mirrors to rotate in two directions and move linearly in one direction. The adjustment accuracy is expected to be 0.03° and 10 μm. The mirrors are later fixed in place with three M1.6 modified titanium screws.

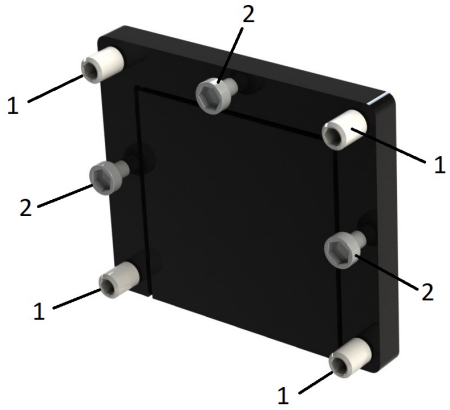

Figure 7: Mirror fine alignment system - fine adjustment screw (1), fixing screw (2).

Image Detection Module

The Image Detection Module is a standalone subsystem of the EOI (Figure 8). It consists of an aluminium housing, the EOI main printed circuit board (PCB), a beamsplitter assembly, two bandpass filters and two sensor assemblies. Due to the high manufacturing complexity and feedback from surface coating companies, an integrated design with the optical solution and sensors mounted in one main body was dropped. Instead, a modular approach was taken. Accurate mounting holes and easy handling were the key considerations when designing this system.

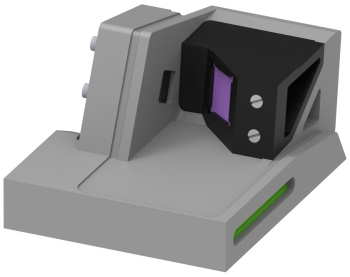

Figure 8: Image Detection Module.

Modularity

A distinctive feature of this system is its ability to be tested without using the main housing with mirrors. This helps to mitigate the risks of harming the optical surfaces and mirrors while running separate non-optics tests on the system. The alignment between the main housing and Image Detection Module is ensured with precise fit and mating surfaces. Another key feature of a modular approach is its easy access to all the subcomponents. The mirrors are mounted to allow adjustments to the primary and tertiary mirrors during image acquisition.

Interfaces

A flex cable connects two identical sensor boards to the main PCB. The actuators, locking mechanism, and feedback sensors are also connected with cables. The precise alignment between the Image Detection Module's aluminium housing and the beam splitter assembly is ensured with grooved mating surfaces and fixed with screws. The filters are firmly held in their mounting holes and supported by the sensor frame.

Shielding

The EOI enclosure and Image Detection Module aluminium housing should protect the electronics from harmful radiation. None of the PCBs have direct radiation exposure.

Outgassing Mitigation

The module's PCBs were purposely separated from the optical channel in the design process. It was done to reduce the risk of the PCBs out-gassing to the mirrors, thus increasing the contamination. Sufficient sealing between the electronics and optical channel is achieved with precise mating edges. All the bolts which need to be glued use a low total mass loss and collected volatile condensable materials space-compatible epoxy-based glue like the Loctite Stycast 2850FT.[19] All the cavities inside the camera have openings with sufficient area for outgassing to eliminate any trapped air after launch.

Calibration Module

The calibration unit consists of a Faulhaber linear actuator,[20] an aluminium frame, a polytetrafluoroethylene (PTFE) guide rail and a diffusive glass. The second calibrator is a shutter. It has the same linear actuator and a similar design to the diffuser. The shutter also covers the diffuser in its storing configuration to protect it from direct sunlight. Both calibrators have a two-level feedback loop for redundancy. The feedback loops are encoders built into the actuators and current measuring power input.

Due to having external linearly moving calibrators, the contact surfaces could not be parallel to the frame because there was no assurance of unwanted light not getting into the optical channel during the calibration cycle. To prevent this, the calibrators and the frame around the aperture are at a 5° angle to make them fit better.

During the launch, both calibrators are locked in their operational position in front of the aperture. This also helps to close the aperture and seal off the optical channel from loose objects and gasses from other parts of the spacecraft or launcher. A spring-loaded lock is released after the satellite is deployed, and the calibrators can move away to their non-operational positions.

The calibrators are supported on both sides to ensure mechanical rigidness for the moving calibrators. This requirement became especially important after choosing the Faulhaber actuators with a tubular rail allowing the calibrator to rotate around its axis. The other end is supported by a profiled guide made out of PTFE. The requirements for the guide material were low outgassing and low wear. The PTFE guide also helped to make the system lubricant-free.

Thermal Analysis

The first analysis was done with all the individual components at extreme temperatures of -40°C and 100°C to determine their maximum von Mises stress and thermal expansion/contraction areas. The initial temperature for all the components was 20°C. The tensile yield strength of 7075-T6 is 503 MPa. The maximum peak stress in all cases exceeds the limit around the attachment points. The analysis

does not consider passive heat transfer between the parts and the satellite. It is to show the worst-case scenario with no heat exchange.

The analysis showed that in both cases, most of the components individually will exceed the limit of elasticity and will have a permanent deformation at thermal limits. This means the thermal limits shall be avoided or handled with thermal control when necessary.

The second analysis considers the space radiation environment. With an expected orbit at the altitude of 650 km, the period is approximately 5864 s. In the operational mode, the EOI is pointed towards the Earth. In this scenario, the total energy from the Sun, with the maximum value of solar flux being 1414 W/m^2 and an average albedo radiation value of 0.3, is 424.2 W/m^2. An average Earth infrared (IR) radiation with such a period is about 240 W/m^2. Making the maximum heat flux in the operational mode 664.2 W/m^2.[21,22]

In the third scenario, as seen in Figure 9, the camera is in calibration mode with the diffuser facing toward the Sun, enabling the camera to be exposed to maximum solar flux. Albedo radiation and Earth IR were considered zero, making the received heat flux equal to the maximum solar flux of 1414 W/m^2.

The results show that during the real worst-case scenario, the main baffle and the main body can withstand the solar flux with minimal surface displacement and elastic deformation. The rear surface and the attachment points need a passive thermal connection to the satellite. To help the mirrors with even heat exchange, a fourth point of contact should be added in the free corner. All the other extremes shall be dealt with by having the proper tolerances.

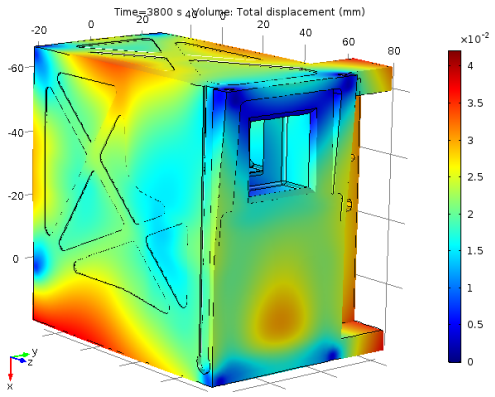

Figure 9: Theia thermal analysis with maximum Sun radiation after 3800 seconds.

Vibration Analysis

During the launch, the EOI witnesses a series of different high and low-frequency random, sine-burst and shock vibrations. The maximum G-forces and frequencies for the analysis were chosen according to Vega C datasheet.[23] The forces reach their highest peak after 3rd stage ignition. The G-forces can go as high as -5 g to +3 g in the longitudinal direction.

For the analysis, a 1.25 times qualification margin will be used. Due to the unknown orientation of the camera during launch, the EOI should withstand random and sine-burst vibrations up to 6.25 g in all directions in the given frequency range. The frequency range in the sine-burst and random vibrations was 5 to 2000 Hz.

The first test with 6.25 g load in each axis showed the maximum displacement, and von Mises stresses in the main structure, as seen in Figure 10. The calibration module was left out of this test for simplicity and limitations in computational power. The calibrators were tested separately. The results showed that all von Mises stress values stayed under 25 kPa, roughly 20 times less than the tensile yield strength of 7075-T6 aluminium.

The second test run was conducted on the diffuser and shutter assemblies. The maximum von Mises stresses observed in this analysis stayed all under 40 kPa, and the displacements stayed under 80 μm making the whole system resilient to sine and random vibrations.

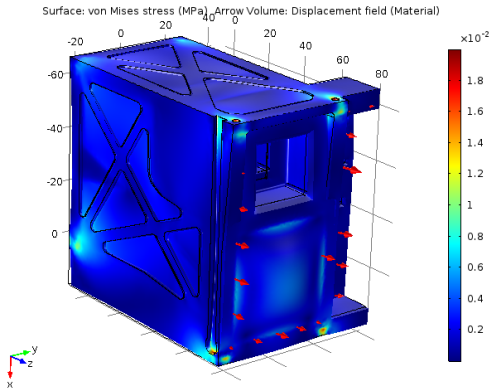

Figure 10: Theia vibration analysis with maximum vibration in Z-axis.

Electronics

The electronics system hosts the main controller and provides communication interfaces and power to the sub-modules, such as the calibration module and optics. The overview in Figure 11 shows the system's topology.

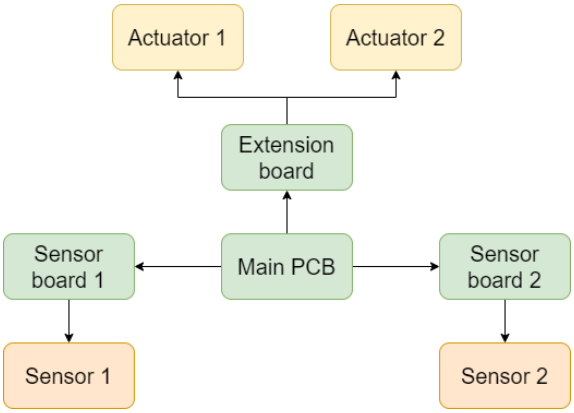

Figure 11: Topology of the electronics

The system consists of three types of PCBs. The main PCB hosts the central STM32H725 microcontroller unit[24] (MCU), which controls the other modules. The sensor PCB, of which two instances are used in the final product, reads images from the sensor and stores them until the main controller requests them. The extension PCB hosts the calibration unit's electronics and connections to external systems.

Main PCB

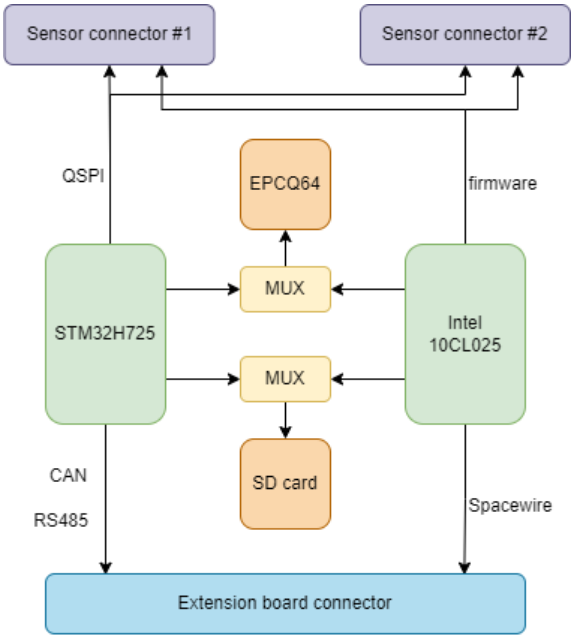

Figure 12: Topology of the main PCB.[25] The main PCB controls the other submodules.

As shown in Figure 12, the main PCB hosts two key processing units: an STM32H725 MCU by STMicroelectronics and an Intel 10CL025 (Cyclone 10 LP) field-programmable gate array (FPGA).[26] The MCU is the central controller of the camera. It handles image processing, controls high-level operations of all FPGAs and saves images to a Secure Digital card (SD card) for long-term storage. In addition, another Cyclone 10 LP FPGA acts as the SpaceWire controller, reading images from the SD card and sending them via the Extension board. It is also responsible for programming the two sensor FPGAs. The three FPGAs are daisy-chained in a single master dual slave configuration. The program memory on the main PCB hosts the firmware for all three FPGAs, which are then automatically programmed when the system is powered on. The program memory can be written to using the MCU or a download cable. Furthermore, there is a debug interface for the MCU and FPGA using Serial Wire Debug (SWD) and Joint Test Action Group (JTAG), respectively.

Extension PCB

The extension PCB hosts the electronics of the calibration unit, which consists of the L6234 brushless direct current motor controller[27] by STMicroelectronics and a multiplexer (MUX) circuit. Since the calibration unit uses two actuators and board space is very limited, the calibration unit controls two actuators using the same control circuit. The MCU controls the multiplexer circuit and selects which actuator is controlled at any given time by multiplexing the three-phase lines.

In addition to the calibration unit, the extension PCB hosts the external interfaces. These are implemented as two D-subminiature-9 (DSUB-9) connectors. One connector is reserved for Spacewire, the other for Controller Area Network (CAN), RS485 and power delivery.

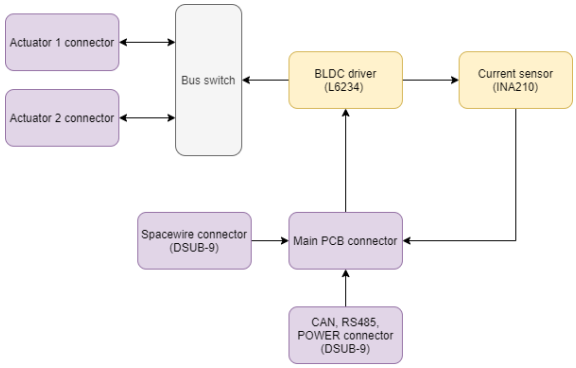

Figure 13: Topology of the extension PCB.[28] The extension PCB connects to external systems and hosts the electronics of the calibration unit.

Sensor PCB

The sensor PCB reads images from the sensor and temporarily stores them in random-access memory (RAM) until the Main MCU requests them. The RAM used is the IS66WVH16M8BLL-166B1LI HyperRAM,[29] which allows reading and writing at a data rate of up to 333 MB/s. The sensor transmits data at a rate of 300 MHz using low-voltage differential signalling (LVDS), which the Cyclone 10 LP FPGA receives. The corresponding LVDS clock is generated by the AD9552BCPZ[30] integrated circuit. The sensor PCB hosts the regulators for various uncommon voltages required for the operation of the sensor. The PCB is connected to the main PCB using a flexible flat cable. The topology of the sensor PCB can be seen in Figure 14.

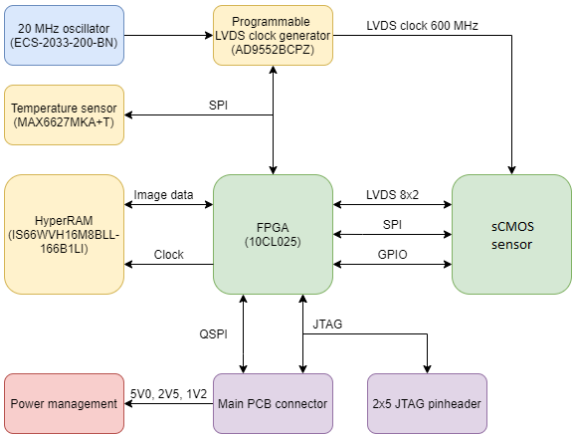

Figure 14: Topology of the sensor PCB.[31,32] The sensor PCB is responsible for the data acquisition from the sCMOS sensor.

Conclusion

This paper presented the optical, mechanical, and electrical designs of a scientific-grade multispectral imager. It was shown that it is feasible for the camera to achieve a radiometric accuracy of 5% and an MTF of 0.13. However, the paper also showed that the MTF of 0.13 is not always necessarily achievable; therefore, possible solutions were presented for increasing the MTF. Furthermore, it was shown through analyses that the camera should survive the launch and space environments. In conclusion, it was demonstrated that it is possible to create a nanosatellite imager to gather quantitative data for remote sensing applications.

Acknowledgments

The European Space Agency has funded this project under the Industry Incentive Scheme and General Support Technology Programme. Moreover, we thank our consultants Tõnis Eenmäe, Joel Kuusk, and Viljo Allik at Tartu Observatory and our technical officer Micael Miranda at ESA. Furthermore, we would like to thank the people who have been part of our team Karin Pai, Mathias Plans, Reimo Soosaar, and Uku Kert Paidra.

References

[1] Joosep Kivastik, Hans Hubert Sams, Silvar Muru, Hendrik Ehrpais, Tõnis Eenmäe, Joel Kuusk, Andris Slavinskis, and Mihkel Pajusalu. Optical design and analysis of Theia: a scientific-grade multispectral imager for nanosatellites. *IEEE Journal on Miniaturization for Air and Space Systems*, 3(4):242–248, 2022.

[2] Thales. Thales alenia space has signed €450 million esa contract to build sentinel-3c and d satellites for copernicus program. `https://www.thalesgroup.com/en/worldwide/space/press-release/thales-alenia-space-has-signed-eu450-million-esa-contract-build`, 2016. [Online; accessed 6 June 2023].

[3] M. Claverie, V. Demarez, B. Duchemin, O. Hagolle, D. Ducrot, C. Marais-Sicre, J.-F. Dejoux, M. Huc, P. Keravec, P. Béziat, R. Fieuzal, E. Ceschia, and G. Dedieu. Maize and sunflower biomass estimation in southwest france using high spatial and temporal resolution remote sensing data. *Remote Sensing of Environment*, 124:844 – 857, 2012.

[4] M. C. Hansen and T. R. Loveland. A review of large area monitoring of land cover change using landsat data. *Remote Sensing of Environment*, 122:66 – 74, 2012. Landsat Legacy Special Issue.

[5] E. K. Melaas, M. A. Friedl, and Z. Zhu. Detecting interannual variation in deciduous broadleaf forest phenology using landsat tm/etm+ data. *Remote Sensing of Environment*, 132:176 – 185, 2013.

[6] S. Lee, A. Hutputanasin, A. Toorian, W. Lan, R. Munakata, J. Carnahan, D. Pignatelli, A. Mehrpavar, and A. Johnstone. CubeSat Design Specification (1U-12U) REV 14.1. `https:`

//static1.squarespace.com/static/5418c831e4b0fa4ecac1bacd/t/62193b7fc9e72e0053f00910/1645820809779/CDS+REV14_1+2022-02-09.pdf, 2022. [Online; accessed 6 June 2023].

[7] NASA Earth Observatory. Normalized Difference Vegetation Index (NDVI). https://earthobservatory.nasa.gov/features/MeasuringVegetation/measuring_vegetation_2.php, 2000. [Online; accessed 6 June 2023].

[8] D. Korsch. *Reflective Optics*. Elsevier, Burlington, MA, USA, 1991.

[9] R. E. Fischer, B. Tadic-Galeb, and P. R. Yoder. *Optical System Design 2nd ed.* Mc Graw Hill, 2008. [doi:10.1036/0071472487].

[10] André Maréchal. *Étude des effets combinés de la diffraction et des aberrations géométriques sur l'image d'un point lumineux...* Éditions de la Revue d'optique théorique et instrumentale, 1948.

[11] European Space Agency. Sentinel-2 MSI Performance. https://sentinel.esa.int/web/sentinel/technical-guides/sentinel-2-msi/performance. [Online; accessed 6 June 2023].

[12] LAMBDARES Research Corporation. OSLO. https://lambdares.com/oslo/. [Online; accessed 6 June 2023].

[13] Acktar Ltd. Acktar Magic Black. https://www.acktar.com/product/magic-black/. [Online; accessed 6 June 2023].

[14] LAMBDARES Research Corporation. TracePro. https://lambdares.com/tracepro/. [Online; accessed 6 June 2023].

[15] M. Drusch, U. [Del Bello], S. Carlier, O. Colin, V. Fernandez, F. Gascon, B. Hoersch, C. Isola, P. Laberinti, P. Martimort, A. Meygret, F. Spoto, O. Sy, F. Marchese, and P. Bargellini. Sentinel-2: Esa's optical high-resolution mission for gmes operational services. *Remote Sensing of Environment*, 120:25 – 36, 2012. The Sentinel Missions - New Opportunities for Science.

[16] Standard for characterization of image sensors and cameras release 4.0. Technical report, European Machine Vision Association, 2021.

[17] ASM Aerospace Specification Metals Inc. Aluminum 7075-T6; 7075-T651. https://asm.matweb.com/search/SpecificMaterial.asp?bassnum=ma7075t6. [Online; accessed 6 June 2023].

[18] Thorlabs, Inc. Hex Adjusters, M2.5 x 0.20 Fine. https://www.thorlabs.com/newgrouppage9.cfm?objectgroup_id=1201. [Online; accessed 6 June 2023].

[19] LOCTITE STYCAST 2850FT CAT 24LV. Technical data sheet, Henkel AG Co. KGaA, 2019.

[20] Linear DC-Servomotors with Analog Hall Sensors - LM 0830 ... 01. Technical data sheet, Dr. Fritz Faulhaber GMBH Co.Kg, 2022.

[21] David G. Gilmore, editor. *Spacecraft Thermal Control Handbook, Volume I: Fundamental Technologies*. The Aerospace Press, 2 edition, 2002.

[22] W. Batts B. J. Anderson. Spacecraft thermal environments. In David G. Gilmore, editor, *Spacecraft Thermal Control Handbook, Volume I: Fundamental Technologies*, chapter 2, pages 21–67. The Aerospace Press, 2002.

[23] Vega C Issue 0 Revision 0. User's manual, Arianespace AS, 2018.

[24] STM32H725xE/G - Arm Cortex-M7 32-bit 550 MHz MCU, up to 1 MB Flash, 564 KB RAM, Ethernet, USB, 3x FD-CAN, Graphics, 2x 16-bit ADCs Rev 3. Datasheet, STMicroelectronics N. V., 2021.

[25] Quad-Serial Configuration (EPCQ) Devices Datasheet. Datasheet, Intel Corporation, 2020.

[26] Intel Cyclone 10 LP Device Datasheet. Datasheet, Intel Corporation, 2022.

[27] L6234 - Three-phase motor driver Rev 11. Datasheet, STMicroelectronics N. V. , 2017.

[28] INA21x Voltage Output, Low- or High-Side Measurement, Bidirectional, Zero-Drift Series, Current-Shunt Monitors. Datasheet, Texas Instruments Incorporated, 2017.

[29] IS66WVH16M8DALL/BLL IS67WVH16M8DALL/BLL - 16M x 8 HyperRAM. Datasheet, Integrated Silicon Solution, Inc., 2020.

[30] Oscillator Frequency Upconverter Rev. E. Datasheet, Analog Devices, Inc., 2009.

[31] ECS-2025/2033 - SMD Clock Oscillator. Datasheet, ECS Inc. International.

[32] MAX6627/MAX6628 - Remote ±1°C Accurate Digital Temperature Sensors with SPI-Compatible Serial Interface Rev 9. Datasheet, Analog Devices, Inc, 2021.